Protein Science (1999), *8*:1292–1304. Cambridge University Press. Printed in the USA.

Study of the stability and unfolding mechanism of BBA1 by molecular dynamics simulations at different temperatures

LU WANG,[1] YONG DUAN,[1] REBECCA SHORTLE,[2] BARBARA IMPERIALI,[3] AND PETER A. KOLLMAN[1]

[1]Department of Pharmaceutical Chemistry, University of California, San Francisco, California 94143
[2]Department of Biochemistry and Biophysics, University of California, San Francisco, California 94143
[3]Department of Chemistry and Chemical Engineering, California Institute of Technology, Pasadena, California 91125

(RECEIVED November 2, 1998; ACCEPTED March 4, 1999)

Abstract

BBA1 is a designed protein that has only 23 residues. It is the smallest protein without disulfide bridges that has a well-defined tertiary structure in solution. We have performed unfolding molecular dynamics simulations on BBA1 and some of its mutants at 300, 330, 360, and 400 K to study their kinetic stability as well as the unfolding mechanism of BBA1. It was shown that the unfolding simulations can provide insights into the forces that stabilize the protein. Packing, hydrophobic interactions, and a salt bridge between Asp12 and Lys16 were found to be important to the protein's stability. The unfolding of BBA1 goes through two major steps: (1) disruption of the hydrophobic core and (2) unfolding of the helix. The β-hairpin remains stable in the unfolding because of the high stability of the type II′ turn connecting the two β-strands.

Keywords: BBA1; energetics; molecular dynamics simulation; protein stability; unfolding mechanism

Understanding protein folding and stability is a long-standing goal of protein chemistry (Jaenicke, 1987; Dill, 1990; Fersht & Serrano, 1993; Matthews, 1993). It is also essential in practical applications such as protein engineering and design (Shaw & Bott, 1996). Generally, to maintain a stable tertiary protein structure without the aid of cross-links like disulfide bonds or metal binding interactions, a natural protein or its domain should have at least 60 residues (Srere, 1984; Goodsell & Olson, 1993). However, recently, this limit has been lowered by several designed or engineered proteins. The villin headpiece domain engineered by McKnight et al. has 36 residues but maintains a tertiary structure consisting of three helices in solution (McKnight et al., 1997). Two other proteins, both designed based on the structure or consensus sequence of zinc fingers, namely, BBA1 (Struthers et al., 1996a) and FSD-1 (Dahiyat & Mayo, 1997), have 23 and 28 residues, respectively, and maintain a similar α/β tertiary fold as a zinc finger in solution. Because of their small size, it is of particular interest to study the forces that stabilize these proteins and the mechanisms by which they fold.

We have performed molecular dynamics simulations on BBA1 and several of its mutants (Struthers et al., 1996a, 1996b, 1998). BBA1 is interesting to study by simulations because it is the smallest protein without disulfide bridges that has a well-defined tertiary structure in solution. BBA1 (Struthers et al., 1996a) was designed based on the consensus sequence of zinc fingers (Berg, 1990) and a particular zinc finger, Zif268 (Pavletich & Pabo, 1991). The protein does not require a zinc ion to be stable in aqueous solution. The solution structure of the protein has been solved by NMR spectroscopy and shares a similar fold to that of a zinc finger (Struthers et al., 1996a). The three-dimensional NMR structure, amino acid sequence, and secondary structure elements of the protein are shown in Figures 1 and 2. Similar to a zinc finger, the tertiary structure of the protein consists of an α-helix and a β-sheet, which arrange like an "L" with an acute angle between them. The major differences between BBA1 and a zinc finger are: (1) The α-helix–β-sheet interface of BBA1 has been designed into a hydrophobic core that helps to stabilize the protein, independent of a zinc ion, while in a zinc finger, a zinc ion is needed at the α-helix–β-sheet interface to stabilize the zinc finger (Frankel et al., 1987; Parraga et al., 1990); (2) the angle between the α-helix and the β-sheet in BBA1 is slightly larger than that of a zinc finger. To maintain its discrete structure, BBA1 still requires two unnatural amino acids (Struthers et al., 1996a): a D-Proline residue at position 4 and a 3-(1,10-phenanthrol-2-yl)-L-alanine (Fen) residue (Fig. 2) at position 6. D-Pro4 and Ser5 form a type II′ turn connecting the two strands of the β-hairpin; the Fen residue is part

Reprint requests to: Peter A. Kollman, University of California, Department of Pharmaceutical Chemistry, Box 0446, Room 101, 513 Parnassus, San Francisco, California 94143-0446; e-mail: pak@cgl.ucsf.edu.

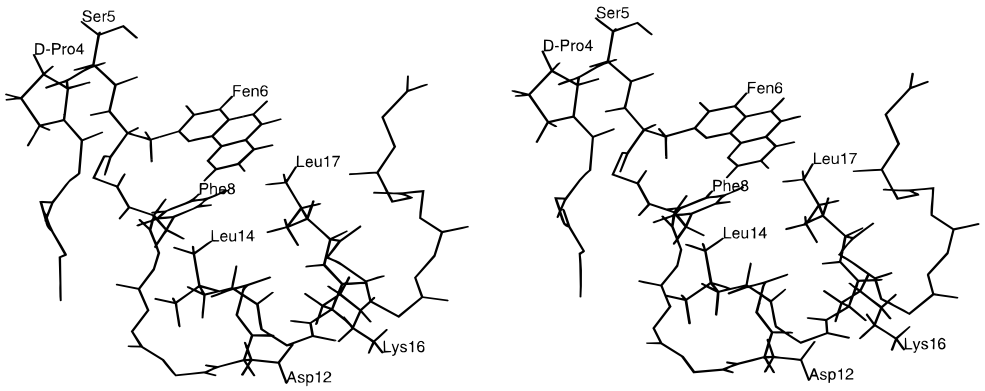

Fig. 1. The structure of BBA1. Only the side chains of D-Pro4, Ser5, Fen6, Phe8, Asp12, Leu14, Lys16, and Leu17 are displayed. Fen6, Phe8, Leu14, and Leu17 are the major residues of the hydrophobic core.

of the hydrophobic core. Experimentally, it was found that the type II′ turn is essential for the stability of the β-hairpin (Struthers et al., 1996b): replacing the type II′ turn with a type II turn by switching the chirality of D-Pro4 and Ser5 to Pro4 and D-Ser5 disrupts the β-hairpin while the helical structure is largely intact. The Fen residue also appears to be important for maintaining the protein's well-defined structure in solution (Struthers et al., 1998): the Fen6 $\rightarrow$ Tyr mutation (BBA2) increases the flexibility of the hairpin and the Fen6 $\rightarrow$ Trp mutation (BBA3) completely disrupts the tertiary structure of the protein. These observations are interesting cases for testing of our simulation methods and force field. However, the Fen residue in BBA1 is not essential for maintaining a well-defined structure; Struthers et al. (1998) have designed variants of BBA1 with a Tyr at position 6 and charged residues at positions 2 and 7, which have NMR structures as well resolved as that of BBA1.

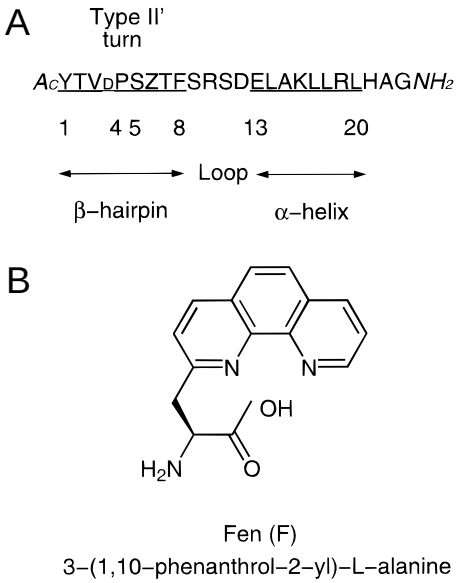

Fig. 2. A: The sequence of BBA1 and the secondary structures. Type II′ turn, 4–5; β-hairpin, 1–8; loop, 9–12; helix, 13–20. "Z" stands for Fen residue. **B:** The chemical structure of Fen residue.

To study the kinetic stability of BBA1 and its mutants, we have performed nanosecond molecular dynamics simulations at different temperatures from 300 to 400 K with explicit representation of solvent. The stability of BBA1 or one of its mutants was estimated from its ability to stay folded as the temperature was raised. In principle, a more quantitative measurement of the stability differences between BBA1 and its mutants can be estimated by calculating their folding free energy differences with the free energy perturbation (FEP) method (Kollman, 1993). However, due to the considerable structural changes involved in the mutations of BBA1, it is difficult to reliably estimate the folding free energy differences with the FEP method, which are accurate only for small structural changes (van Gunsteren, 1989; Kollman, 1993). In addition, the unfolding simulations provide us with an opportunity to characterize the protein's unfolding pathways. As an extension to such an approach, calculations of the folding free energy landscape have been attempted (Boczko & Brooks, 1995) using unfolding simulations. Such calculations may yield valuable information but are computationally expensive because they require extensive sampling at the relevant conformations and connecting regions. For a qualitative understanding of the kinetic stability, as we will demonstrate later, much can be learned through unfolding simulations. Hirst and Brooks (1995) applied such methods in the study of the stabilities of fragments of apomyoglobin.

The subsequent sections are organized as follows. In the first part of Results, we analyze the stability of BBA1 and its mutants by carrying out simulations at different temperatures. Particularly, we will test our simulation methods and force field by comparing our simulation results with the experimental observations on BBA1, BBA2, BBA3, and the mutant with the II′ turn $\rightarrow$ II turn mutation at positions 4–5. We also analyze the stability of several other mutants to study the influence of packing interactions and salt bridges, and discuss the influence of long-range interactions on the simulation results. In the second part of Results, we analyze the unfolding of BBA1 at 380 and 400 K. The unfolding pathway has been characterized in terms of changes in global structure, secondary structure content, solvent accessible area, and native contacts. In Discussion, we analyze the possible energetic bases of the stability differences between BBA1 and its mutants. We also discuss the unfolding mechanism of BBA1 and comment on the limitations of unfolding simulations. In Conclusion, we briefly summarize the results.

Materials and methods

Model and force field

The NMR structure of BBA1 was solved by Struthers et al. (1998). The structures of the mutants were generated by model building using standard geometry based on the coordinates of BBA1. The atomic charges of the Fen residue were calculated by fitting the electrostatic potential around the dipeptide model, Ace-Fen-NMe, using the RESP method (Bayly et al., 1993). Here "Ace" and "NMe" stand for acetyl and N-methylamide groups, respectively. The electrostatic potential was obtained by a single point ab initio quantum mechanical calculation using Gaussian94 (Frisch et al., 1995) with a 6-31G* basis set on the geometry generated by energy minimization of the dipeptide with the AM1 method. The side-chain dihedral of Fen was chosen to be in an extended conformation, with the side-chain dihedral χ (N-C_α-C_β-C_γ) $\cong 180°$. Most of the bond, angle, and dihedral parameters of Fen were available in the AMBER force field. The missing parameters were assigned the values of similar types in the force field (Table 1).

Simulation procedures

The molecular dynamics (MD) simulations and energy minimization were performed with the SANDER module of the AMBER4.1 program (Pearlman et al., 1995) using periodic boundary conditions (Allen & Tildesley, 1989). Two sets of force fields were tested, parm94, reported by Cornell et al. (1995) and parm96, reported by Kollman et al. (1997), which differ only in the ϕ and ψ torsional potentials. Eventually, parm96 was used for most of the simulations. BBA1 or one of its mutants was placed at the center of a box of $45 \times 45 \times 45$ Å^3 filled with TIP3P water molecules (Jorgensen et al., 1983) under standard conditions; the number of water molecules was ~2,660. One Cl^- counterion was placed near Arg19 to maintain the neutrality of the system. The time step of the MD simulations was 2 fs. The pressure (1 atm) and the temperatures of the systems were controlled by Berendsen's method (Berendsen et al., 1984). In all cases, an 8 Å cutoff radius was used, either for the simulations with or without applying the Particle-Mesh Ewald (PME) method (Darden et al., 1993) to include the contributions of long-range interactions. For the PME calculations, we used a 1 Å grid size and the fourth order B-spline interpolation to calculate the potential and forces in between grid points. To improve simulation efficiency, only those bond lengths involving hydrogen atoms were constrained with the SHAKE algorithm (Ryckaert et al., 1977). Each MD simulation was about 1 ns and prior to each simulation, the system was energy minimized for 500 steps and equilibrated for about 5 ps. All the simulations were performed on the CRAY T3E machine at the Pittsburgh Supercomputing Center.

Table 1. *The angle and improper dihedral parameters of Fen that are not available in AMBER 4.1*[a]

Angle or dihedral	K_f	n	θ_0
CA-CA-NC	70.0		122.8
CT-CA-NC	70.0		117.2
CB-CB-CB	70.0		122.7
CA-CB-CA	70.0		125.4
HA-CA-NC	35.0		117.2
CA-CB-CB-CA	1.1	2	180.0
CB-NC-CB-CB	1.1	2	180.0
NC-CA-CA-CT	1.1	2	180.0
CA-CA-CB-CB	1.1	2	180.0
CB-CB-CB-NC	1.1	2	180.0

[a]CB, carbon atoms connecting two rings in Fen; CA, other carbon atoms in the aromatic rings; HA, hydrogen atoms attached to CA. The angle potential is $E_a = K_f(\theta - \theta_0)^2$. The improper dihedral potential is $E_d = K_f[1 + \cos(n\theta - \theta_0)]$. K_f is in kcal/(mol deg^2) for the angles and kcal/mol for the improper dihedrals. θ_0 is in degrees.

Analyses of MD trajectories

For each simulation, the root-mean-square deviations (RMSDs) of the trajectories recorded at 5 ps interval were calculated for the backbone atoms C_α, N, C and, O with reference to the starting structure at $t = 0$. Only residues 1–20 were considered in the calculations because the C-terminal of the helix (residues 21–23) was frayed and quite flexible in the molecular dynamics simulations. The experimentally determined structure indicated that the C-terminal was only frayed at residue 23. The RMSDs were calculated after optimal superimposition of the coordinates to remove translational and rotational motion (Kabsch, 1976). The structure at $t = 0$ was used as the reference rather than the NMR structure of BBA1, because the RMSDs better represented the structural changes in the simulations. The $t = 0$ structures of the simulations, which were generated from short equilibration, generally had very similar folds to that of the native structure with RMSD $\leq$ 2 Å.

Because the absolute values of dihedrals cannot be defined uniquely, direct calculation of the average backbone dihedrals ($\langle\phi\rangle$ and $\langle\psi\rangle$) of residues along the MD trajectories may give unreasonable results. Instead, we used the vector average method from circular statistics (Batschelet, 1981) to calculate the average dihedrals. Each dihedral θ was expressed as a unit vector $\mathbf{a}_i = \cos\theta\,\mathbf{e}_x + \sin\theta\,\mathbf{e}_y$. The vector sum of the dihedrals, $\sum\mathbf{a}_i$, was normalized and expressed as $\mathbf{a}_m = \cos\theta_m\mathbf{e}_x + \sin\theta_m\mathbf{e}_y$. θ_m was used to represent the average dihedral and does not depend on the definition of the sign and zero point of individual θ's. Once $\mathbf{a}_m$ was determined, we calculated the angles between each vector $\mathbf{a}_i$ with $\mathbf{a}_m$ simply from their dot products, and the fluctuation of the angles was used as the fluctuation of the dihedrals around the mean dihedral.

The secondary structure contents (helix, sheet, and other) were calculated with the Kabsch–Sander algorithm (Kabsch & Sander, 1983) implemented in the MidasPlus package (Ferrin et al., 1988). The default hydrogen bonding energy criterion of -0.5 kcal/mol was used.

The solvent accessible areas (SAAs) of the structures were calculated by the Boolean logic method (Le Grand & Merz, 1993). Essentially, each atom surface (with a radius of van der Waals (VDW) radius + the probe radius) was represented by dots with a given density; the area was calculated as number of dots $\times$ dot density. Subtracting the dots in the overlapping area between atoms from the total number of dots of all atoms in the system yields the solvent accessible areas. The dot density used in our calculations was 3.0/Å^2. The probe radius was 1.4 Å.

To calculate the native contact percentage of a given structure, first, the number of contacts in the native structure N_0 was calculated. Two residues are considered to be in contact if any heavy

atom (C, N, O, S) of one residue is within 4.5 Å from any heavy atom of the other residue (Daggett & Levitt, 1993). Contacts between neighboring residues (i and $i + 1$) were excluded. Second, the contacts N_1 were counted for the given structure, but for the same contact pairs in the native structure. The native contact percentage of the given structure is $N_1/N_0 \times 100\%$.

Results

The stability of BBA1 and its mutants

In the following, we use BBA1′ to denote the BBA1 mutant that has a type II turn at positions 4–5 (D-Pro4 → L-Pro & L-Ser5 → D-Ser mutations). BBA2 and BBA3 represent the mutants of Fen6 → Tyr and Fen6 → Trp, respectively. Other mutants are represented by their residue changes. For example, Fen6 → Ala is the BBA1 mutant that has Fen → Ala mutation at position 6.

Parm94 vs. Parm96

Recently, it was shown that modification of the dihedral potentials of ϕ (C-N-Cα-C) and ψ (N-Cα-C-N) of the peptide backbone in parm94 (Cornell et al., 1995), which led to parm96 (Kollman et al., 1997), gave a conformational energy profile of alanine tetrapeptide that was in better agreement with high level ab initio calculations. The effect of the modification is that in parm96, the relative stability of β-sheet vs. α-helix is more favorable for the β-sheet than in parm94 (Kollman et al., 1997). We have performed several test simulations with both parm94 and parm96 on BBA1 and BBA2 at 300 K. The RMSDs in the time course of the simulations are shown in Figure 3. Both parm94 and parm96 give low RMSDs for BBA1, indicating that the structure is stable in the simulations. However, for BBA2 with parm94, the RMSD increases to about 6 Å at 1 ns, indicating that the structure is not stable in the simulation. Since experimentally, it was found that both BBA1 and BBA2 have comparable tertiary folds at 300 K (albeit, BBA1 has better defined NMR spectra), we used parm96 for all our simulations. By examining the structure of BBA2 at t = 1 ns with parm94, we found that the β-hairpin of the protein has unfolded. The increased stability of β structures in parm96, therefore, is important to the stability of the β-hairpin.

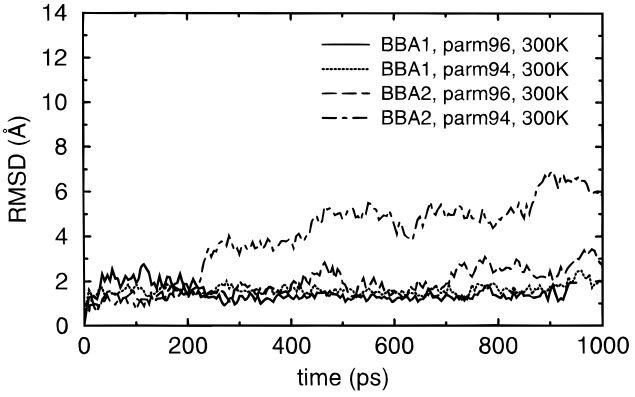

Fig. 3. The RMSDs of BBA1 and BBA2 simulated with parm94 and parm96 at 300 K using an 8 Å cutoff.

BBA1, BBA2, and BBA3

The RMSDs in the time course for the proteins simulated at different temperatures are shown in Figure 4. For BBA1 (Fig. 4A), at 300 and 360 K, the RMSDs of the trajectories remain around 2 Å (the average is slightly less than 2 Å), indicating that the structure is stable at these temperatures in the simulations. At 380 K, the RMSD increases to beyond 2 Å at about 350 ps and reaches about 5 Å at t = 1 ns. The structure at t = 1 ns is unfolded (Fig. 5A). However, the secondary structures seem intact. At 400 K, the RMSD increases to 8.5 Å at t = 450 ps, but goes down to 5 Å at t = 1 ns. If one prolongs the simulation, the RMSD goes up again to 7.8 Å at t = 1.4 ns.

Similar to BBA1, BBA2 remains stable in the unfolding simulations at 360 K (Fig. 4B), and its RMSD is about 2 Å at t = 1 ns and the average RMSDs are around 2 Å at 300 and 360 K. At 380 K, the RMSD remains almost constant around 1.5 Å until ~700 ps and then goes up to 3 Å at t = 1 ns. Although the RMSD is not large, the structure has clearly unfolded (Fig. 5B). At 400 K, the RMSD increases after about 400 ps and reaches 7 Å at t = 1 ns. Since the unfolding of BBA2 at 380 or 400 K is slower than that of BBA1, it appears that BBA2 is kinetically more stable than BBA1 in the simulations. However, it should be noted that this kinetic stability might not necessarily reflect the thermodynamic stability, which is determined by the free energy difference between the folded and unfolded states of a protein. This issue will be discussed further below.

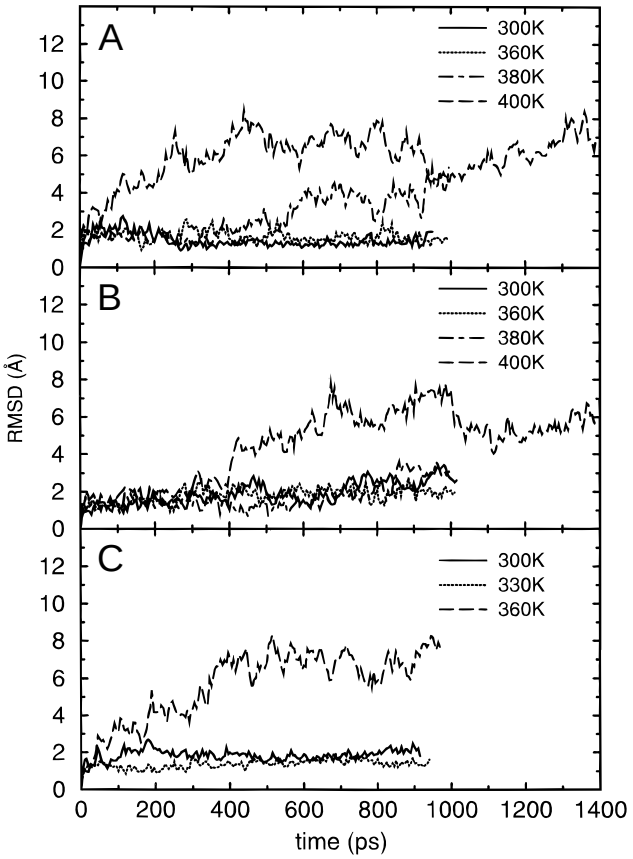

Fig. 4. The RMSDs of BBA1, BBA2, and BBA3 simulated at different temperatures. **A:** BBA1. **B:** BBA2. **C:** BBA3.

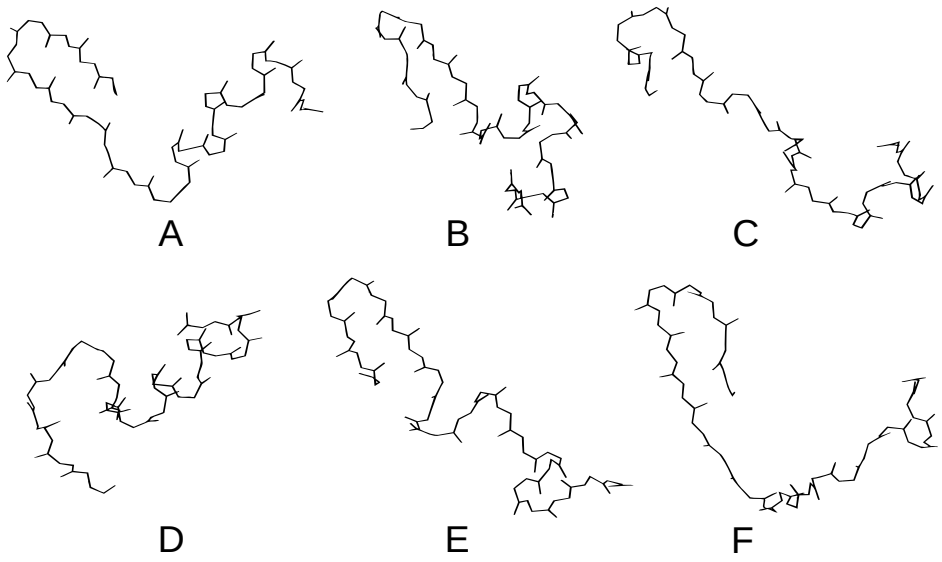

Fig. 5. The unfolded structures at $t = 1$ ns for BBA1 and its mutants. **A:** BBA1, 380 K. **B:** BBA2, 380 K. **C:** BBA3, 360 K. **D:** BBA1′, 330 K. **E:** Fen6 → Ala, 300 K. **F:** Asp12 → Ala and Lys16 → Ala, 330 K.

Compared with BBA1 and BBA2, BBA3 appears to be less stable (Fig. 4C). In the simulations, BBA3 is stable at 300 and 330 K, as is indicated by a low RMSD around or below 2 Å at 300 and 330 K. But, at 360 K, the RMSD quickly increases and reaches about 8 Å at the end of the simulation. The end structure is unfolded (Fig. 5C).

Experimentally, it was found that BBA1 has a well-defined structure in NMR, but BBA2 and BBA3 do not. Circular dichroism experiments (B. Imperiali, unpubl. data) lead to similar curves as a function of temperature for BBA1, BBA2, and BBA3, but they may be dominated by the presence of the α-helix. Our simulated unfolding kinetic stability of BBA1, BBA2, and BBA3 suggests that BBA1 and BBA2 have comparable kinetic stability, and BBA3 has less kinetic stability. The NMR data of BBA1 were sharp and well defined, whereas broadened signals were observed for those residues near residue 6 for BBA2 (7–10). For BBA3, broadening was observed at all residues and was particularly extreme for residues 1–12 (Struthers et al., 1998). We have calculated the backbone dihedral fluctuations (BDFs) of BBA1, BBA2, and BBA3 at 300 and 360 K and the results are presented in Figure 6. At 300 K, all have comparable and low BDFs, although, surprisingly, BBA3 has the lowest BDF. At 360 K, the trend is in reasonable agreement with the experiment: BBA2 has a higher BDF than BBA1, in the loop region and in the helix; BBA3 has the highest BDF in a broad region from the loop to most part of the helix. The BDFs at the end of the helix are high. This is because the end of the helix is frayed in the simulations. For this reason, we only used residues 1–20 to calculate the backbone RMSDs of the trajectories.

A key design strategy of BBA1 was the inclusion of a tight type II′ turn at positions 4–5 (Struthers et al., 1996b). Because of its intrinsic stability in solution, the turn is likely to be a structural nucleation element of folding (Struthers et al., 1996b). Indeed, we found the turn to be stable in the simulations, even at the unfolding temperatures. The average backbone dihedrals of the turn residues of BBA1, BBA2, and BBA3 are all close to the standard dihedrals of a type II′ turn, and the fluctuations of the dihedrals are insensitive to temperature (Table 2). The BDFs of Ser5 are larger than those of Pro4, apparently due to the rigidity of Pro residue backbone.

BBA1′

If the type II′ turn is replaced by a type II turn (BBA1′) by simply changing the chirality of D-Pro4 and L-Ser5, at 300 K, the

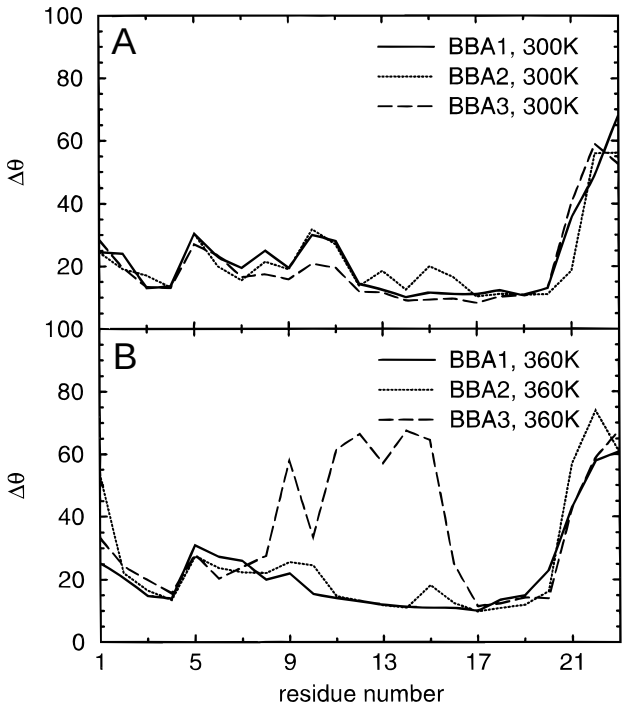

Fig. 6. The BDFs of BBA1, BBA2, and BBA3, simulated at (**A**) 300 K and (**B**) 360 K.

Table 2. *The average backbone dihedrals and their fluctuations (in degrees) of the type II′ turn (D-Pro4, L-Ser5) of BBA1, BBA2 and BBA3 in the simulations*[a]

	BBA1	BBA2	BBA3
300 K	62 ± 11	60 ± 11	60 ± 10
	−121 ± 16	−119 ± 16	−121 ± 15
	−87 ± 27	−98 ± 30	−85 ± 23
	3 ± 35	13 ± 32	4 ± 31
360 K	62 ± 11	61 ± 11	60 ± 11
	−119 ± 17	−119 ± 16	−114 ± 21
	−91 ± 27	−84 ± 28	−97 ± 30
	−1 ± 35	−4 ± 28	2 ± 27
400 K	62 ± 12	63 ± 13	
	−118 ± 19	−114 ± 20	
	−102 ± 29		
	−104 ± 31		
	11 ± 30	2 ± 40	
Standard type II′ turn[b]		60	
		−120	
		−80	
		0	

[a] For each case, the four dihedral values and their fluctuations are those of the ϕ,ψ of D-Pro4 and ϕ,ψ of L-Ser5, respectively.
[b] From Sibanda and Thornton (1985).

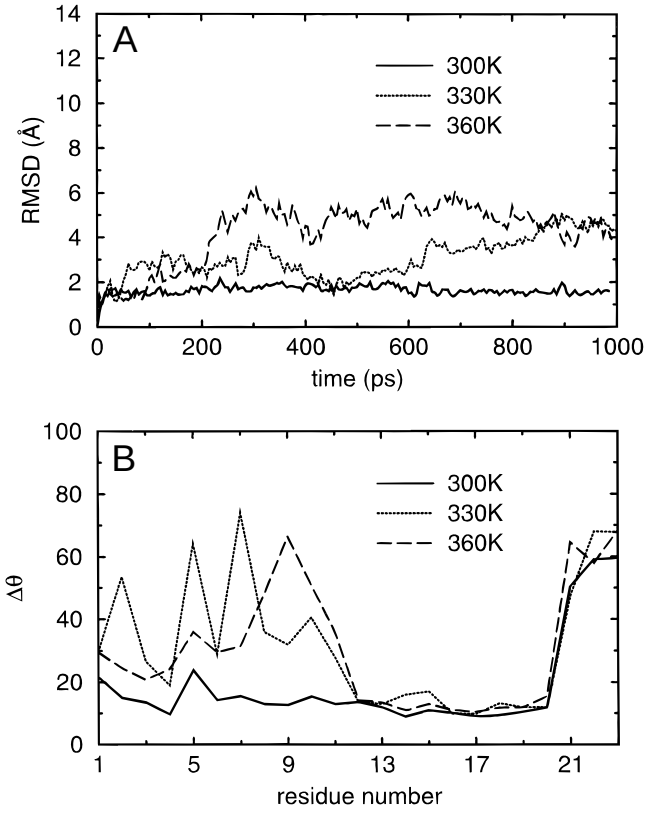

Fig. 7. The (**A**) RMSDs and (**B**) BDFs of BBA1′ simulated at 300, 330, and 360 K.

protein unfolds but interestingly, the helical part is largely intact (Struthers et al., 1996b). We have model built the structure of BBA1′ and performed MD simulations on BBA1′ at 300, 330, and 360 K.

At 300 K, BBA1′ is stable in the simulation with an almost constant RMSD around 1.6 Å (Fig. 7A). At 330 K, the RMSD fluctuates considerably in the beginning of the simulation and increases to 4.3 Å at $t = 1$ ns. Inspection of the structure at $t = 1$ ns indicates that the β-hairpin has unfolded, but the helix is intact (Fig. 5D). This unfolded structure clearly agrees with the experimental observation. At 360 K, the RMSD increases to 6 Å in 300 ps and then fluctuates and reaches 4.3 Å at $t = 1$ ns.

The BDFs and the average backbone dihedrals in the turn and helix region of BBA1′ at 300, 330, and 360 K are shown in Table 3 and Figure 7B. As the temperature is raised, the BDFs in the β-hairpin and loop region increase significantly, while the fluctuations in the helix region remain low. The average backbone dihedrals of the helix region at the three temperatures indicate that the helix part remains helical. The BDFs at 330 K in the β-hairpin and loop regions are larger than those at 360 K. We propose that the hairpin unfolds quickly at 360 K, indicating a low kinetic barrier, and remains in a relatively stable minimum after unfolding, suggesting a kinetic trap in the vicinity of the (partially) unfolded state. Similarly, the BDFs of D-Ser5 are larger than those of L-Pro4 because L-Pro4 is more rigid. Interestingly, at 360 K, $\langle\psi\rangle$ of D-Ser5 has shifted from around zero to a quite negative value (−118°), while the other average dihedrals of the turn stay close to the ideal values of type II turn. This indicates that as the temperature is raised, there is a conformational change associated with the change in the ψ dihedral of D-Ser5, accompanying by the β-hairpin unfolding.

Fen6 → Ala, Phe8 → Ala, and Leu17 → Ala

Since Fen6, Phe8, and Leu17 are at the center of the hydrophobic core of BBA1, it is of interest to mutate each one of these residues into an alanine residue and see their influences on the protein's stability. The results are shown in Figure 8.

Table 3. *The average backbone dihedrals (in degrees) of BBA1′ in the turn (4–5) and helix regions (12–20) at 300, 330, and 400 K*[a]

	300 K	330 K	360 K
Turn			
Pro4	−46, 110	−66, 140	−64, 123
Ser5	84, 8	88, −3	96, −118
Helix			
Glu13	−70, −42	−69, −42	−70, −41
Leu14	−62, −45	−62, −42	−59, −45
Ala15	−55, −44	−60, −43	−57, −42
Lys16	−51, −49	−52, −50	−54, −49
Leu17	−54, −54	−54, −50	−57, −50
Leu18	−58, −46	−58, −46	−57, −43
Arg19	−57, −48	−59, −45	−55, −47
Leu20	−59, −51	−57, −47	−61, −49

[a] For each residue, the two dihedral values are the average ϕ and ψ, respectively.

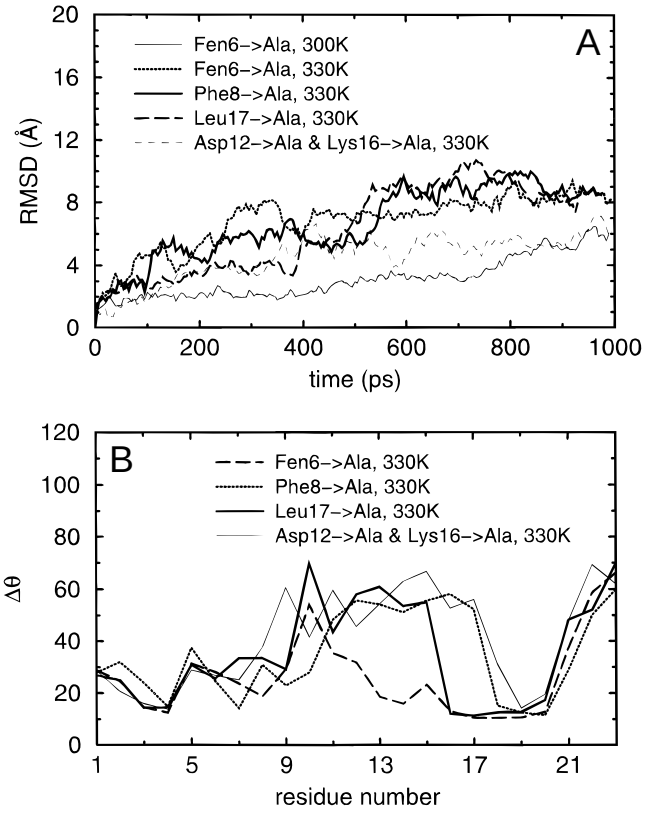

Fig. 8. A: The RMSDs of Fen6 → Ala, Phe8 → Ala, Leu17 → Ala, and Asp12 → Ala and Lys16 → Ala. **B:** The BDFs of Fen6 → Ala, Phe8 → Ala, Leu17 → Ala, and Asp12 → Ala and Lys16 → Ala.

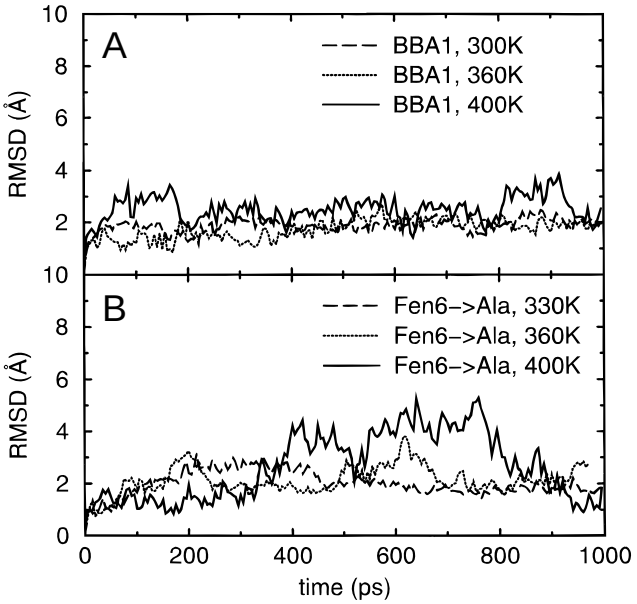

Fig. 9. A: The RMSDs of BBA1 simulated at 300, 360, and 380 K with PME. **B:** The RMSDs of Fen6 → Ala simulated at 330, 360, and 380 K with PME.

All the mutations result in destabilization of the protein. The mutant Fen6 → Ala is unstable at 300 K, as indicated by a slow increase in RMSD after 400 ps and a RMSD of about 4 Å at 1 ns (unfolded, see Fig. 5E); at 330 K, the RMSD of the mutant increases from the beginning of the simulation and reaches 6 Å at t = 1 ns. Phe8 → Ala and Leu17 → Ala are unstable at 330 K and their RMSDs are 6.4 and 5.3 Å, respectively, at t = 1 ns. All the mutants have large BDFs in the loop regions (Fig. 8B), and there are large BDFs in the helix region as well in Phe8 → Ala and Leu17 → Ala mutants.

Asp12 → Ala/Lys16 → Ala

The salt bridge formed by Asp12 and Lys16 at the N-terminal of the helix may provide a capping interaction that stabilizes the helix. Although the mutation of the two charged residues into two alanine residues does not alter the hydrophobic core, it can reduce the stability of the N-terminal helix next to the loop region, and the resulting increase of flexibility in the loop region may decrease the stability of the protein. To test the hypothesis, we performed the simulation on the mutant Asp12 → Ala/Lys16 → Ala at 330 K.

The mutant is indeed found to be unstable. The RMSD (Fig. 8A) of the mutant increases shortly after the simulation starts and reaches 6.1 Å at t = 1 ns (the unfolded structure is shown in Fig. 5F). The BDF also indicates that there are large fluctuations in the loop region and in most parts of the helix (Fig. 8B).

The influence of long-range interactions

In all the above simulations, we used a cutoff radius of 8 Å, which does not include the contributions of long-range interactions. This should be appropriate because most of our mutations are nonpolar in nature, for which short-range interactions dominate. We also expect the simulation of Asp12 → Ala/Lys16 → Ala with 8 Å to be a reasonable approximation because the two charged groups are close in space and the total charge is zero. In particular, BBA1 is stable in the simulation at 300 K with an 8 Å cutoff. This provides the basis for comparing the stability of BBA1 and its mutants. So far, the results of our simulations with 8 Å cutoff are in qualitative agreement with the available experimental observations. However, it is important to study the influence of long-range interactions on the simulation results. We have performed the simulations with PME (Darden et al., 1993) for two cases, BBA1 and Fen6 → Ala.

With long-range interactions included by PME, both BBA1 and Fen6 → Ala become kinetically more stable compared with the corresponding cutoff simulations (Fig. 9). With PME, even at 400 K, BBA1 is still quite stable with its RMSD fluctuating around 2.5 Å, although the RMSDs are larger than those at 300 and 360 K. This is in contrast with the unfolding of BBA1 at 400 K in the cutoff simulation. With PME, Fen6 → Ala is stable until 360 K and becomes unstable at 400 K, as is indicated by a large fluctuation in RMSD. In the cutoff simulation Fen6 → Ala had been unstable at 300 K and rapidly unfolded at 330 K. From the simulations with PME, we can still see that BBA1 is more stable than Fen6 → Ala, but the difference is smaller than that in the cutoff simulations. Therefore, with long-range interactions included, it is more difficult to differentiate the stability of BBA1 and Fen6 → Ala. Presumably these owe partly to the time frame of our simulations. One may expect that with PME unfolding would occur at extended simulation time scale that is in contrast to the relatively short time needed to unfold the proteins in the cutoff simulations. This is consistent with the fact that the PME, with the inclusion of long-

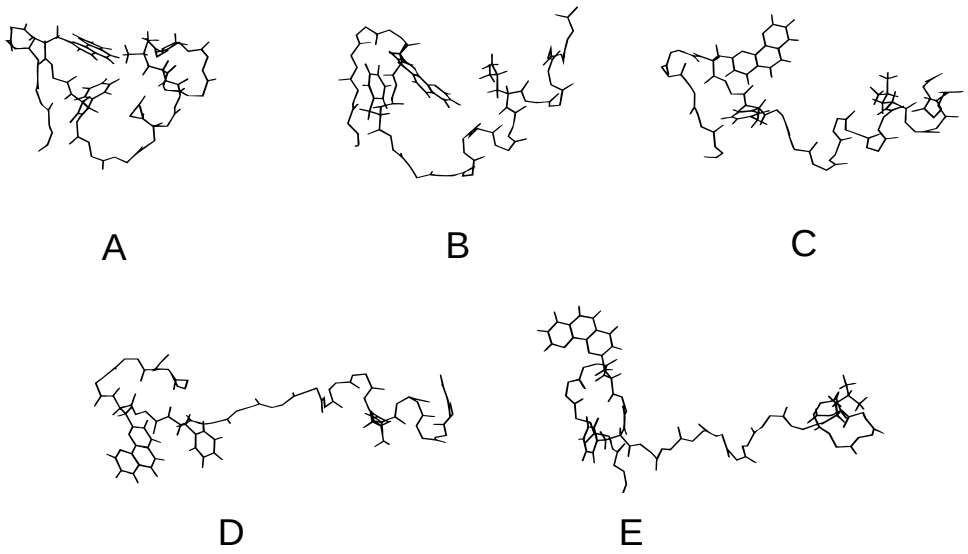

Fig. 10. A: The structure of BBA1 at $t = 0$, 40, 540, and 940 ps in the unfolding simulation at 380 K. **B:** The structure of BBA1 at $t = 0$, 45, 95, 330, and 1,210 ps in the unfolding simulation at 400 K. Only the side chains of Fen6, Phe8, and Leu17 are shown.

range electrostatic interactions, represents the interactions accurately. The cutoff, on the other hand, is less accurate than PME in the representation of the energetic surface and inevitably introduces noise and effectively elevates the simulation temperature and makes it possible to reveal the unfolding process within a shorter simulation time scale.[4]

It should be noted that the use of 8 Å cutoff in the simulations is only appropriate for comparing the stability of mutants that differ mainly in short-ranged interactions. As a necessary condition for a proper comparison, the native structure must be stable in the simulation with 8 Å cutoff at room temperature. This may not work for systems with many charged groups. For example, we later found that BBA5 (Fen6 → Tyr, Thr2 → Arg, and Thr7 → Asp), which has two additional charged groups compared with BBA1 and a well-defined tertiary structure at 300 K (Struthers et al., 1998), was not stable in the simulation at 300 K with 8 Å cutoff (data not shown). Only with 10 Å cutoff does BBA5 become stable in the simulation at 300 K. Therefore, for a proper comparison of the stability of BBA5 and BBA1 and other mutants, it appears that at least 10 Å cutoffs have to be used. These comparisons involve simulations requiring significantly more computer time and were not pursued in this study. It is noted that the two charged residues at positions 2 and 7 in BBA5 may not be necessary for maintaining its well-defined tertiary structure. In BBA6, Asp7 was replaced with the polar neutral asparagine and in BBA7, Arg2 was replaced by a serine. Both BBA6 and BBA7 have well-defined tertiary structures in solution (Struthers et al., 1998). The contribution of charged or polar amino acids at positions 2 and 7 appears to be the destabilization of undesired conformations rather than a particularly stabilizing interaction across the hairpin (Struthers et al., 1998).

[4]The noise due to truncation to the electrostatic interactions can be viewed as additional energy to the system and the temperature coupling may remove part of such effect. The truncation may also reduce the energy barriers hence reduce the time needed to cross the barriers.

The unfolding mechanism of BBA1 at 400 K

The small size of BBA1 makes it a particularly interesting system for studying protein folding mechanisms. For comparison, we have examined the unfolding processes of BBA1 at 380 and 400 K.

Description of the unfolding process

From the trajectories, we found that the unfolding of BBA1 at 380 and 400 K both consist of the following two basic steps (Fig. 10). First, the hydrophobic core was dissolved as the helix and the β-hairpin gradually separated from each other. Second, the hydrophobic core further opened up and structure became extended. Before the hydrophobic core fell apart, the Fen residue first protruded into the hydrophobic core between Phe8 and Leu17, which might have helped to pry open the hydrophobic core. The protrusion of the Fen residue into the hydrophobic core happened early, at $t = 40$ ps and $t = 45$ ps, respectively, in the 380 and 400 K simulations. The opening of the hydrophobic core occurred at $t = 590$ ps at 380 K and at an earlier time of $t = 95$ ps at 400 K. There were still some tertiary contacts in the loop region after the hydrophobic core had opened up. These tertiary contacts were disrupted at $t = 940$ ps at 380 K and at $t = 330$ ps at 400 K. At 400 K, the helix then remained stable until $t = 1{,}230$ ps when it further unfolded. The β-hairpin was stable in the unfolding processes both at 380 K and at 400 K.

Native contacts

The native contact percentages in the unfolding processes are shown in Figure 11A. The unfolding at 380 K does not have a significant change in native contact percentage. But it is clear that at $t \approx 500$ ps there is decrease in native contact percentage, corresponding to opening of the hydrophobic core and at $t \approx 950$ ps, there is a further decrease in native contact percentage, corresponding to disruption of the tertiary contacts in the loop region. The change of native contact percentage in the unfolding at 400 K is more dramatic. The decrease of native contact percentage at

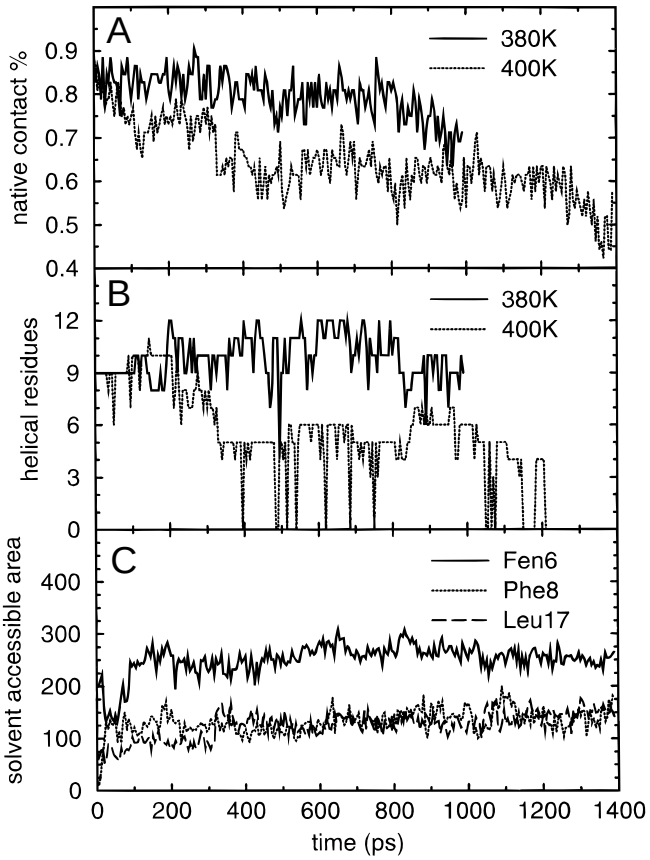

Fig. 11. The changes of native contact percentage, number of helical residues and solvent accessible area (in Å^2) in the unfolding simulations of BBA1. **A:** The native contact percentages. **B:** The number of helical residues. **C:** The solvent accessible areas of Fen6, Phe8, and Leu17 in the 400 K simulation.

$t \approx 100$ ps signals the opening of the hydrophobic core. The drop in native contact percentage at $t \approx 300$ ps represents the unfolding of the contacts in the loop region, which lead to the unfolding of the N-terminus of the helix. At $t \approx 1{,}200$ ps, the native contact percentage further decreases and corresponds to the further unfolding of the helix. The contact maps of the structures at $t = 0$, 95, 330, and 1,210 ps in the 400 K simulation (Fig. 12) convey the same messages as the native contact percentage but with more detailed structural information. At $t = 0$, the contacts in the upper right and lower left represent the helix and the β-hairpin, respectively. The contacts in the middle represent the loop and the hydrophobic core. At $t = 95$ ps, clearly, some contacts in the loop and the β-hairpin are disrupted, corresponding to the opening of the hydrophobic core. At $t = 330$ ps, more contacts in the loop have disappeared and concurrently, the contacts in the helix region decrease, corresponding to unfolding of the N-terminal region, while the contacts in the β-hairpin remain roughly unchanged. At $t = 1{,}210$ ps, there is further decrease of contacts in the helix, corresponding to further unfolding.

Secondary structure contents

The helix contents in the simulations are shown in Figure 11B. Although there are considerable fluctuations, the trends are clear. At 380 K, the overall helix contents remain high, in agreement with the results from inspection of the trajectories. At 400 K, there is a two-stage change in the process. The first dramatic decrease in the number of helical residues occurred at $t \approx 300$ ps, corresponding to the unfolding of helix in the N-terminal region. The second dramatic decrease in the number of helical residues happened at $t \approx 1{,}200$ ps, corresponding to the further unfolding of the helix. It is noted that the fluctuations in the calculated number of helical residues are due to the Kabsch and Sander algorithm (Kabsch & Sander, 1983) that is based on the hydrogen-bonding criteria. This algorithm should be more precise for determining helix contents than those methods based on the dihedral criteria, but is more sensitive to structural fluctuations. For the 380 and 400 K simulations, the number of sheet residues were found to be always around 6, which is the maximum number of sheet residues in the β-hairpin, excluding the two turn residues. This indicates that the β-hairpin is stable during the unfolding simulations.

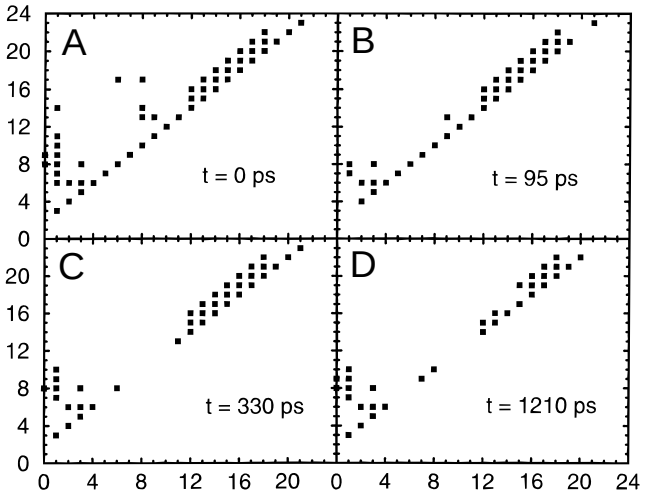

Fig. 12. The contact map of BBA1 at $t = 0$, 95, 330, and 1,210 ps in the unfolding simulation at 400 K.

Solvent accessible area

As expected, the solvent accessible area (SAA) of BBA1 increased during the unfolding simulations. We have found that for the 380 K simulation, SAA started at 2,400 Å^2, increased to 2,800 Å^2, and then did not change much until the end of the simulation. For the 400 K simulation, SAA started similarly at 2,400 Å^2, increased slowly only after 500 ps, and reached 2,800 Å^2 at the end of the simulation. The SAAs of those residues in the hydrophobic core should increase as the protein is unfolded, and they are exposed to solvent. As an example, the SAAs of Fen6, Phe8, and Leu17 in the 400 K simulation are shown in Figure 11C. Indeed, their SAAs all increased during the unfolding process. Interestingly, the SAA of Fen6 decreases considerably in the initial unfolding process and then increases. The decrease in SAA should correspond to the intrusion of Fen6 into the hydrophobic core between Phe8 and Leu17.

Discussion

Why are the stabilities of BBA1, BBA2, and BBA3 different?

The simulations suggest that BBA3 is less stable than BBA1 and BBA2, and that BBA2 appears to be slightly more stable than

Table 4. *The interaction energies (kcal/mol) of residue 6 with the rest of system in BBA1, BBA2, and BBA3*[a]

Protein	Residue	Interaction energy
BBA1	Fen6	−156.1
BBA2	Tyr6	−159.0
BBA3	Trp6	−146.6

[a]The interaction energies were calculated on the energy minimized structures of BBA1, BBA2, and BBA3. The cutoff radius is 8 Å.

BBA1 in the unfolding simulations. Such a specific ordering of the stability lacks correlation with the number of aromatic rings presented in the residue that is somewhat counterintuitive because Fen, Tyr, and Trp are all aromatic residues and BBA1, BBA2, and BBA3 have three, one, and two aromatic ring(s), respectively. For a qualitative analysis, we have calculated the interaction energies of the Fen6, Trp6, or Tyr6 residue with the rest of the protein and solvent, using the corresponding energy minimized structures (Table 4). In agreement with the stability trend observed in the unfolding simulations, Tyr6 has the lowest interaction energy, Fen6 has the second lowest interaction energy, and Trp6 has the highest interaction energy, which is higher than those of Tyr6 and Fen6 by 12.4 and 9.5 kcal/mol, respectively. Such an ordering of the interaction energies (Trp6 > Fen6 > Tyr6) is not correlated with the sizes of the side chains (Fen6 > Trp6 > Tyr6) notwithstanding the fact that the interaction energy is an inherent extensive quantity. Thus, the stability differences are most likely due to the packing interaction differences in the structures. The packing of Fen6, Tyr6, and Trp6 are shown in Figure 13. One sees that the packing of Fen6 and Tyr6 are compact, while the packing of Trp6 is not. The reason may be that Trp6 has a five-membered ring that has to be placed perpendicular to the ring of Phe8 for optimal packing. The same problem does not occur for Fen6 and Tyr6, which have six-membered rings, which can pack parallel to the ring of Phe8. This 5-member ring vs. 6-member ring difference may be the primary packing difference between Fen6 or Tyr6 and Trp6. The packing difference between Fen6 and Tyr6 is likely more subtle.

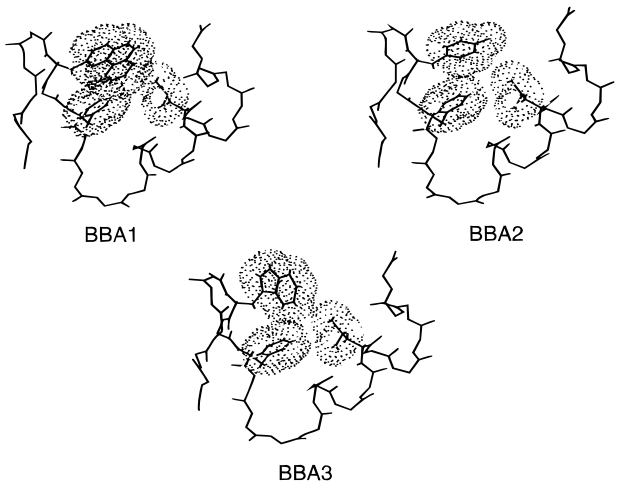

Fig. 13. The packing interactions of Fen6, Tyr6, and Trp6 in BBA1, BBA2, and BBA3.

Why is the II′ turn more stable than the II turn?

The simulations have demonstrated that a type II turn at position 4–5 leads to an unstable β-hairpin while a type II′ turn at the same position leads to a stable β-hairpin. It is of particular interest to analyze the energetic basis of this stability difference. Statistical analyses on protein structures have found that among tight turns, there are more type II′ turns than type II turns (Sibanda & Thornton, 1985). Modeling building based on rigid standard geometry suggests that a type II′ turn will result in a convergent β-hairpin, while a type II turn will result in a divergent β-hairpin (Sibanda & Thornton, 1985). The energetic basis of this difference is not clear. The stability difference between the two turns should be determined by their interaction energies with the rest of the system (protein and water) and their intra-turn energies. For the simulations of BBA1 and BBA1′ at 300 K, we found that the average total energies of the two terms are -485.3 ± 8.7 and -485.0 ± 11.5 kcal/mol, respectively, which cannot rationalize the stability difference. Instead, we propose the following mechanism. Shown in Figure 14 are the structures of BBA1 (type II′ turn) and BBA1′ (type II turn) around the turn region. For both turns, H_6 and O_3 form a hydrogen bond that holds the turn structure in place. For BBA1′, O_4 is above the plane of the turn and H_5 is below the plane. The H_6-O_4 and H_6-H_5 interactions together will tend to open up the turn because the H_6-O_4 distance will decrease while the H_6-H_5 distance will increase to lower the interaction energy. Because the β-hairpin is right-handed twisted, as is common in protein structures (Chothia, 1973; Richardson, 1981) and can be rationalized on energetic terms (Chou et al., 1983; Wang et al., 1996), the tendency of opening the turn up will be enhanced due to the twist because their movements are in the same direction. The result will be a flipping around the dihedral of N_5-$C_{\alpha 5}$-C_5-N_6. That is exactly what was observed in the simulations of BBA1′, in which the ψ (N_5-$C_{\alpha 5}$-C_5-N_6) of Ser5 has shifted from around zero to a negative value during the unfolding of the β-hairpin. On the other hand, for BBA1 (type II′ turn), O_4 is below the plane of the turn and H_5 is above the plane. Similarly, the H_6-O_4 and H_6-H_5 interactions will tend to open up the turn, but it is easy to see that this tendency will be opposed by the right-handed twist of the β-hairpin. For these reasons, a type II′ turn at position 4–5 may be more stable than a type II turn.

It should be noted that the discussion presented above is based on the observations of unfolding simulations in which the turns are part of protein structures. Further studies may be needed to address the issue quantitatively using free energy calculations (Anderson & Hermans, 1988; Tobias & Brooks, 1991) such as WHAM (Kumar et al., 1992) and FEP (Kollman, 1993) that is beyond the scope of present study.

The role of hydrophobic interactions and salt bridges in the protein's stability

The mutations of Fen6 → Ala, Phe8 → Ala, and Leu17 → Ala all lead to instability of the protein in the simulations. Because the hydrophobicities of Phe, Leu, and very likely, Fen, are higher than Ala (Nozaki & Tanford, 1971), these results demonstrate that hydrophobic interactions are important to the stability of the protein. The instability of the mutants is closely related to the high flexibility in the hydrophobic core. This high flexibility is obviously a

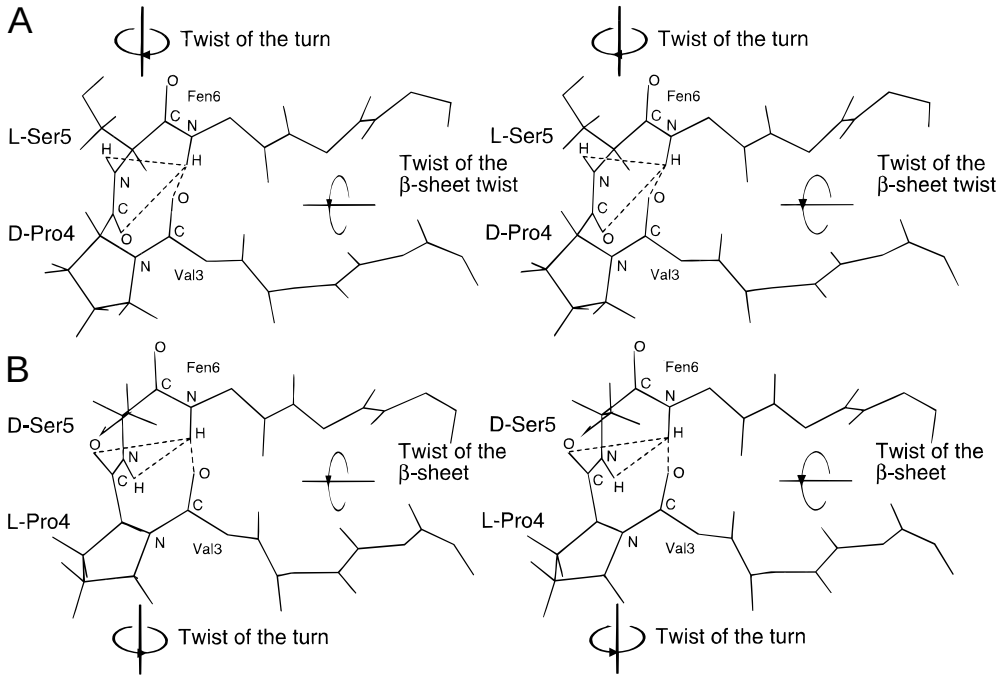

Fig. 14. The twisting interactions in the type II′ turn of BBA1 and in the type II turn of BBA1′. Only the side chains of residues 4 and 5 are shown.

result of shortening of the side chain of Fen6, Phe8, or Leu17, which may weaken the packing interactions in the hydrophobic core. Thus, in addition to the reductions in hydrophobic interactions, weakening of packing interactions may also contribute to the instabilities of the mutants. The mutation of the salt bridge, Asp12 → Ala and Lys16 → Ala, does not directly reduce the interactions in the hydrophobic core because the salt bridge is on the surface of the protein. Rather, it decreases the stability of the N-terminus of the helix near the hydrophobic core.

The unfolding mechanism of BBA1

The unfolding simulations of BBA1 at 380 and 400 K indicate that the unfolding process consists of two major steps: (1) disruption of the hydrophobic core and (2) further unfolding of the structure. For the 380 K simulation, the second step did not involve further disruption of the secondary structure, while for the 400 K simulation, step (2) involved further unfolding of the helix. Similar processes have been found in previous molecular dynamics unfolding simulations of other proteins (Daggett & Levitt, 1993; Tirado-Rives & Jorgensen, 1993; Li & Daggett, 1996), although those proteins are much larger in size than BBA1. However, there are several special features in the unfolding of BBA1. In the unfolding at 380 K, the helix did not unfold even after the hydrophobic core was dissolved. In the unfolding at 400 K, the helix unfolded, not immediately after the opening of the hydrophobic core, but after the native contacts in the loop region next to the N-terminal region of the helix were disrupted. This suggests that native contacts in the loop region stabilize the helix. These contacts may well provide some favorable capping interactions (Presta & Rose, 1988) to the helix because Asp12 and Ser11 are both good capping residues in the N-terminus of a helix (Richardson & Richardson, 1988). The complete unfolding of the helix took a long time (from t = 330 to 1,210 ps), indicating the high stability of the helix. Indeed, it has been found experimentally that the helix is stable at room temperature (Struthers et al., 1996b). The β-hairpin appears to be even more stable because during the unfolding simulations at 380 and 400 K, the β-hairpin actually does not unfold. This should be attributed to the intrinsic high stability of the type II′ turn at residues 4–5. Given the stability of both the helix and the β-hairpin, we speculate that the folding of BBA1 at room temperature would start from the formation of the helix and the β-hairpin (Kim & Baldwin, 1982) followed by the formation of the tertiary structure.

Limitations of unfolding simulations

In this study, unfolding simulations were performed to study the relative kinetic stabilities of BBA1 and its mutants as well as the unfolding mechanism of BBA1. The simulations were not able to rationalize why BBA2 had a broader and less well-determined NMR spectra than BBA1 although the lower kinetic stability calculated for BBA3 compared with BBA1 or BBA2 is consistent with its significantly broader NMR spectra. However, there is not necessarily a one to one correspondence between the sharpness of NMR spectra and the relative kinetic or thermodynamic stability. Nonetheless, we generally found a fairly good correlation between the relative kinetic stabilities in the 1 ns simulations at various temperatures of different mutants and the experimentally observed rigidity or amount of order of the protein structures. For this reason, our unfolding simulations seem useful for analyzing relative protein stabilities and unfolding pathways. In our simulations, a cutoff of 8 Å was used. This did not work for BBA5, which has more charged residues than other mutants. For BBA5, a cutoff of 10 Å had to be used to maintain a stable tertiary structure at 300 K.

The inclusion of more accurate long-range interactions through PME increases the kinetic stability presumably by reducing the electrostatic "noise" in the atomic forces. Thus, with limited computer power, if the goal is to study and understand protein unfolding, the less accurate cutoff model may be appropriate provided that one can show that it leads to stable structure in control simulations (e.g., BBA1 at 300 K). We have presented data to suggest that our unfolding simulations have value as an empirical method which may provide useful insights, as can be seen also from previous unfolding simulations (Daggett & Levitt, 1993; Tirado-Rives & Jorgensen, 1993; Caflisch & Karplus, 1994). For characterizing the unfolding pathway, unfolding simulation with one or a few starting coordinates at least can be used to capture the major features of the real unfolding process, because it has been shown that unfolding simulations with different starting coordinates may share some common features (Lazaridis & Karplus, 1997). This is possible because although protein dynamics are inherently chaotic (Zhou & Wang, 1996; Braxenthaler et al., 1997), which makes individual unfolding trajectories unpredictable in a time course, the unfolding of a protein may still be within a patch of well-defined phase space (Zhou & Wang, 1996; Braxenthaler et al., 1997). In principle, an unfolding process cannot be used to represent a folding process unless the folding and unfolding are reversible. Therefore, to best understand the folding mechanism from an unfolding simulation, the unfolding conditions should be as mild as possible. Because of the small size of BBA1 and its mutants, we were able to gradually increase the simulation temperatures and unfold the proteins at very low temperatures (380 and 400 K). From this point of view, our unfolding simulations have an advantage in realism over previous unfolding simulations that used much higher unfolding temperatures (Daggett & Levitt, 1993; Tirado-Rives & Jorgensen, 1993; Caflisch & Karplus, 1994).

A referee has suggested that multiple simulations at a given temperature are required to establish that our results are not anecdotal; we disagree. The simulations reported in this study were conducted at various temperatures for each structure, including room temperature, below, around, and above unfolding temperatures. The change of simulation temperature in our simulations ensures that the simulations are independent and provides an important test on the consistency of the results. Furthermore, the fact that these independent simulations (Figs. 3, 4A–C, 7A, 8A, 9A, 9B) give sensible and clear trends supports their internal consistency.

Conclusion

We have studied BBA1 and its mutants by molecular dynamics simulations at various temperatures. Using the force field parm96 (Kollman et al., 1997), the simulations were able to qualitatively rank most of the relative stabilities of the mutants studied. The simulations also provided insights into the forces that stabilize the protein. Hydrophobic and packing interactions and a salt bridge between Asp12 and Lys16 were found to be important to the protein's stability. In agreement with experiment, the stability of a type II′ turn and the instability of a type II turn at position 5–6 were observed in the simulations. A mechanism for the stability and instability of the two types of turns were proposed, in which the stability difference was attributed to the different electrostatic interactions in the two types of turns. The analyses of the unfolding process of BBA1 at 380 and 400 K indicate that the unfolding processes consist of two major steps: (1) disruption of the hydrophobic core and (2) further unfolding of the structure. Because the helix and the β-hairpin have considerable stability during the unfolding simulations, we speculate that the folding of BBA1 at room temperature would proceed by the formation of the secondary structures and followed by the tertiary structure formation (Kim & Baldwin, 1982).

Acknowledgment

This work has been supported by NIH (Grant GM-29072) and a University of California Biotechnology Star grant from AMGEN (to P.A.K.). Supercomputing time was provided by Pittsburgh Supercomputer Center (PSC). The facilities of the UCSF computer graphics laboratory, supported by NIH P41-RR01081, T. Ferrin, principal investigator, are gratefully acknowledged. R.S. acknowledges the support of a Department of Defense ONR predoctoral fellowship.

References

Allen MP, Tildesley DJ. 1989. *Computer simulations of liquids*. Oxford, United Kingdom: Clarendon Press.

Anderson AG, Hermans J. 1988. Microfolding: Conformational probability map for the alanine dipeptide in water from molecular dynamics simulation. *Proteins 3*:262–265.

Batschelet E. 1981. *Circular statistics in biology*. New York: Academic Press, Inc.

Bayly CI, Cieplak P, Cornell WD, Kollman PA. 1993. A well behaved electrostatic potential base method using charge restraints for deriving atomic charges: The RESP model. *J Phys Chem 97*:10269–10280.

Berendsen HJC, Postma JPM, van Gunsteren WF, DiNola A, Haak JR. 1984. Molecular dynamics with coupling to an external bath. *J Comp Phys 81*:3684–3690.

Berg JM. 1990. Zinc finger domains: Hypotheses and current knowledge. *Annu Rev Biophys Biophys Chem 19*:405–421.

Boczko EM, Brooks CL III. 1995. First-principles calculation of the folding free-energy of a 3-helix bundle protein. *Science 269*:393–396.

Braxenthaler M, Unger R, Auesbach D, Geven JA, Moult J. 1997. Chaos in protein dynamics. *Protein 29*:417–425.

Caflisch A, Karplus M. 1994. Molecular-dynamics simulation of protein denaturation—Solvation of the hydrophobic cores and secondary structure of barnase. *Proc Natl Acad Sci USA 91*:1746–1750.

Chothia C. 1973. Conformation of twisted β-pleated sheets in proteins. *J Mol Biol 75*:295–302.

Chou K-C, Nemethy G, Scheraga HA. 1983. Role of inter-chain interactions in the stabilization of the right-handed twist of β-sheets. *J Mol Biol 68*:389–407.

Cornell WD, Cieplak P, Bayly CI, Gould IR, Kenneth J, Merz M, Ferguson DM, Spellmeyer DC, Fox T, Caldwell JW, Kollman PA. 1995. A second generation force field for the simulation of proteins, nucleic acids, and organic molecules. *J Am Chem Soc 117*:5179–5197.

Daggett V, Levitt M. 1993. Protein unfolding pathways explored through molecular dynamics simulations. *J Mol Biol 232*:600–619.

Dahiyat BI, Mayo SL. 1997. De novo protein design: Fully automated sequence selection. *Science 278*:82–87.

Darden T, York D, Pedersen L. 1993. Particle Mesh Ewald—An N·log(n) method for Ewald sums in large systems. *J Chem Phys 98*:10089–10092.

Dill KA. 1990. Dominant forces in protein folding. *Biochemistry 29*:7133–7155.

Ferrin TE, Huang CC, Jarvis LE, Langridge R. 1988. The MIDAS display system. *J Mol Graph 6*:13–27.

Fersht AR, Serrano L. 1993. Principles of protein stability derived from protein engineering experiments. *Current Opinion in Structural Biology 3*:75–83.

Frankel AD, Berg JM, Pabo CO. 1987. Metal-dependent folding of a single zinc finger from transcription factor IIIA. *Proc Natl Acad Sci 84*:4841.

Frisch MJ, Trucks GW, Schlegel HB, Gill PMW, Johnson BG, Robb MA, Cheeseman JR, Keith T, Petersson GA, Montegomery JA, Rahavachari K, Al-Laham MA, Zakrzewski VG, Ortiz JV, Foresman JB, Peng CY, Ayala PY, Chen W, Wong MW, Andres JL, Replogle ES, Gomperts R, Martin RL, Fox DJ, Binkley JS, Defrees DJ, Baker J, Stewart JP, Head-Gordon M, Gonzalez C, Pople JA. 1995. Gaussian 94, Revision B.3. Pittsburg, Pennsylvania: Gaussian Inc.

Goodsell DS, Olson AJ. 1993. Soluble proteins: Size, shape and function. *Trends Biochem Sci 18*:65–68.

Hirst JD, Brooks CL III. 1995. Molecular dynamics simulations of isolated helices of myoglobin. *Biochemistry 34*:7614–7621.

Jaenicke R. 1987. Folding and association of proteins. *Prog Biophys Mol Biol 49*:117–237.
Jorgensen WL, Chandrasekhar J, Madura JD, Impey RW, Klein ML. 1983. Comparisons of simple potential functions for simulating liquid water. *J Chem Phys 79*:926–935.
Kabsch W. 1976. A solution for the best rotation to relate two sets of vectors. *Acta Cryst A32*:922–923.
Kabsch W, Sander C. 1983. Dictionary of protein secondary structure: Pattern recognition of hydrogen bonded and geometrical features. *Biopolymers 22*:2577–2637.
Kim PS, Baldwin RL. 1982. Specific intermediates in the folding reactions of small proteins and the mechanism of protein folding. *Ann Rev Biochem 59*:631–660.
Kollman PA. 1993. Free energy calculations: Applications to chemical and biological phenomena. *Chem Rev 93*:2395–2417.
Kollman PA, Dixon RW, Cornell WD, Fox T, Chipot C, Pohorille A. 1997. The development/application of a "minimalist" organic/biochemical molecular mechanic force field using a combination of *ab initio* calculations and experimental data. In: van Gunsteren WF, ed. *Computer simulations of biological systems*. Dordrecht, The Netherlands: ESCOM.
Kumar S, Bouzida D, Swendsen RH, Kollman PA, Rosenberg JM. 1992. The weighted histogram analysis method for free energy calculations on biomolecules: I. The method. *J Comp Chem 13*:1011–1021.
Lazaridis T, Karplus M. 1997. "New view" of protein folding reconciled with the old through multiple unfolding simulations. *Science 278*:1928–1931.
Le Grand SM, Merz KM. 1993. Rapid approximation to molecular-surface area via the use of boolean logic and look-up tables. *J Comp Chem 14*:349–352.
Li A, Daggett V. 1996. Identification and characterization of the unfolding transition state of chymotrypsin inhibitor 2 by molecular dynamics simulations. *J Mol Biol 257*:412–429.
Matthews BW. 1993. Structural and genetic analysis of protein stability. *Ann Rev Biochem 62*:139–60.
McKnight CJ, Matsudaira PT, Kim PS. 1997. NMR structure of the 35-residue villin headpiece subdomain. *Nat Struct Biol 4*:180–184.
Nozaki Y, Tanford CH. 1971. The solubility of amino acids and two glycine peptides in aqueous ethanol and dioxane solutions. *J Biol Chem 246*:2211–2217.
Parraga G, Horvath S, Hood L, Young ET, Klevit RE. 1990. Spectroscopic studies of wild-type and mutant "zinc finger" peptides: Determinants of domain folding and structure. *Proc Natl Acad Sci USA 87*:137–141.
Pavletich NP, Pabo CO. 1991. Zinc finger-DNA recognition: Crystal structure of a Zif268-DNA complex at 2.1 Å. *Science 252*:809–817.
Pearlman DA, Case DA, Caldwell JW, Ross WS, Cheatham TEI, Ferguson DM, Seibel GL, Singh UC, Weiner PK, Kollman PA. 1995. AMBER. San Francisco: University of California.
Presta LG, Rose GD. 1988. Helix signals in proteins. *Science 240*:1632–1641.
Richardson JS. 1981. The anatomy and taxonomy of protein structure. *Adv Protein Chem 34*:167–339.
Richardson JS, Richardson DC. 1988. Amino acid preferences for specific locations at the ends of alpha helices. *Science 240*:1648–1652.
Ryckaert J-P, Ciccotti G, Berendsen HJC. 1977. Numerical integration of the cartesian equations of motion of a system with constraints: Molecular dynamics of n-alkanes. *J Comp Phys 23*:327–341.
Shaw A, Bott R. 1996. Engineering enzymes for stability. *Curr Opin Struct Biol 6*:546–550.
Sibanda BL, Thornton JM. 1985. Beta-hairpin families in globular proteins. *Nature 316*:170–174.
Srere PA. 1984. Why are enzymes so big? *Trends Biochem Sci 9*:387–390.
Struthers MD, Cheng RP, Imperiali B. 1996a. Design of a monomeric 23-residue polypeptide with defined tertiary structure. *Science 271*:342–345.
Struthers MD, Cheng RP, Imperiali B. 1996b. Economy in protein design—Evolution of a metal-independent β–β–α motif based on the zinc finger domains. *JACS 118*:3073–3081.
Struthers MD, Ottesen JJ, Imperiali B. 1998. Design and NMR analyses of compact, independently folded BBA motifs. *Folding Design 3*:95–103.
Tirado-Rives J, Jorgensen WL. 1993. Molecular-dynamics simulations of the unfolding of apomyoglobin in water. *Biochemistry 32*:4175–4184.
Tobias DJ, Brooks CL III. 1991. Thermodynamics and mechanism of alpha helix initiation in alanine and valine peptides. *Biochemistry 30*:6059–6070.
van Gunsteren WF. 1989. Methods for calculation of free energies and binding constants: Successes and problems. In: van Gunsteren WF, Weiner PK, eds. *Computer simulations of biomolecular systems*. Leiden: ESCOM. pp 27–59.
Wang L, O'Connell T, Tropsha A, Hermans J. 1996. Molecular simulations of β-sheet twisting. *J Mol Biol 262*:283–293.
Zhou HB, Wang L. 1996. Chaos in biomolecular dynamics. *J Phys Chem 100*:8101–8105.